Journal of Power Sources 248 (2014) 83–90

Contents lists available at ScienceDirect

Journal of Power Sources

journal homepage: www.elsevier.com/locate/jpowsour

Effect of porosity heterogeneity on the permeability and tortuosity of gas diffusion layers in polymer electrolyte membrane fuel cells

Aydin Nabovati [a], James Hinebaugh [b], Aimy Bazylak [b,*], Cristina H. Amon [a]

[a] Advanced Thermal/Fluids Optimization, Modelling and Simulation (ATOMS) Laboratory, Department of Mechanical & Industrial Engineering, University of Toronto, 5 King's College Road, Toronto, Ontario, Canada M5S 3G8
[b] Thermofluids for Energy and Advanced Materials (TEAM) Laboratory, Department of Mechanical & Industrial Engineering, University of Toronto, 5 King's College Road, Toronto, Ontario, Canada M5S 3G8

HIGHLIGHTS

- Stochastic, 3D carbon fiber material models generated with controlled porosity heterogeneity.
- Lattice Boltzmann method employed to measure bulk hydrodynamic properties.
- Porosity heterogeneity contributed a negligible effect on modeled transport, compared to porosity and material composition.
- Tortuosity increases with binder & PTFE fraction, which was unexpected by the authors.
- Permeability increases with permeability and binder & PTFE fraction.

ARTICLE INFO

Article history:
Received 23 June 2013
Received in revised form
1 September 2013
Accepted 15 September 2013
Available online 24 September 2013

Keywords:
Porosity heterogeneity
Binder & PTFE
Permeability
Tortuosity
Gas diffusion layer
Lattice Boltzmann method

ABSTRACT

In this paper, we study the effect of porosity heterogeneity on the bulk hydrodynamic properties (permeability and tortuosity) of simulated gas diffusion layers (GDLs). The porosity distributions of the heterogeneous reconstructed samples are similar to those previously reported in the literature for Toray TGP-H 120™ GDLs. We use the lattice Boltzmann method to perform pore-level flow simulations in the reconstructed GDL samples. Using the results of pore-level simulations, the effect of porosity distribution is characterized on the predicted in- and cross-plane permeability and tortuosity. It was found that porosity heterogeneity causes a higher in-plane permeability and lower in-plane tortuosity, while the effect is opposite in the cross-plane direction, that is a lower cross-plane permeability and a higher cross-plane tortuosity.

We further investigate the effect of adding poly-tetra-fluoro-ethylene (PTFE) & binder material to the reconstructed GDL samples. Three fiber volume percentages of 50, 75, and 100% are considered. Overall, increasing the fiber volume percentage reduces the predicted in- and cross-plane permeability and tortuosity values. A previously reported relationship for permeability of fibrous materials is fitted to the predicted permeability values, and the magnitude of the fitting parameter is reported as a function of fiber volume percentage.

1. Introduction

Hydrogen-based power systems, specifically fuel cells, have attracted significant attention in the last decade due to their low local CO_2 emission, high efficiency, and versatility. Among different types of fuel cells, polymer electrolyte membrane (PEM) fuel cells, which typically have energy conversion efficiencies over 50%, are a promising option for the transportation sector, distributed power generation, and backup power generation, to name a few applications [1–4].

Considerable advancements have been made towards the commercial development of PEM fuel cells in areas such as reduced platinum loading, higher current density, and reduced costs; however, there still exist challenges that should be removed before PEM fuel cells can become commercially viable. Mass transport issues such as liquid water flooding at high current working conditions leads to inefficient performance [5]. Overcoming these operational challenges requires more research on characterization and performance-evaluation of PEM fuel cell materials, which will

* Corresponding author. Tel.: +1 416 946 5031; fax: +1 416 978 7753.
E-mail address: abazylak@mie.utoronto.ca (A. Bazylak).

0378-7753/$ – see front matter © 2013 Elsevier B.V. All rights reserved.
http://dx.doi.org/10.1016/j.jpowsour.2013.09.061

inform new material designs for improved efficiency and product reliability.

Computational modeling, next to experimental studies, has been widely used to study mass, energy, and charge transport at different length scales inside PEM fuel cells. The numerical studies can be categorized into two groups, namely: (i) studies that use first principles, thus, can only include small system sizes comparable to length scales of the transport phenomenon under study, and (ii) studies that use models and relations to predict transport phenomena inside multiple components of a fuel cell, and predict the cell-level behavior. These models usually include larger combined domains, and need effective transport properties of each part of the cell as an input. The aim of many of the works under the first category is to predict effective transport properties of individual components of a PEM fuel cell, which will be used in the studies of the second type.

One particular part of a PEM fuel cell, which is the focus of this paper, is the gas diffusion layer (GDL). The GDL is a layer consisting of carbon fibers in either woven or non-woven formats. The thickness of a GDL is typically between 200–400 μm, with fiber diameters in the range of 7–10 μm. In a conventional PEM fuel cell, the GDL is placed between the micro porous layer (MPL) and a graphite plate that includes gas channels. The produced water inside the cell passes through the GDL to be guided out of the system via gas channels. The GDL should be of overall high thermal and electrical conductivity, and should be structured in a way that prevents excess water accumulation.

The GDL influences many aspects of a PEM fuel cell's operation, thus, accurate prediction of its effective transport properties is crucial in understanding the cell performance. El-Kharouf et al. [6] presented a comprehensive review of available ex-situ measurement techniques for determining a range of GDL properties.

A review of available methods for bulk porosity measurement techniques is presented by Cindrella et al. [7]. Determining effective thermal conductivity of GDL samples has also been subject of many previous studies [8–13]. Another important bulk transport property of a GDL is its absolute permeability. Bulk permeability prediction in GDL samples has been widely investigated numerically and experimentally [14–19]. All these works focus on determining the bulk permeability, and do not discuss the effect of pore-level structural parameters on the permeability. Recently, Fishman et al. [20] showed that porosity distribution through the thickness of GDL samples is not uniform. Through rigorous analysis of computed tomography (CT) scan images of samples from different manufacturers, they reported typical porosity distribution profiles of different types of GDLs. In another work, Fishman and Bazylak [21] studied the effect of poly-tetra-fluoro-ethylene (PTFE) and binder material addition on the overall through-thickness porosity profiles of GDL samples. They reported that PTFE and binder material accumulate in low porosity areas, where the density of fibers is higher.

It is known that the heterogeneous porosity distribution affects the overall transport properties of porous material [22,23], however, this dependance has not been quantified. Fishman et al. [24] applied the available relations for permeability/tortuosity of porous materials to the measured porosity profile inside the GDL, and mapped the porosity profile into permeability/tortuosity profiles. In this work, we show that their method of calculating the resultant bulk permeability is only accurate for the in-plane direction.

In this work, we use pore-level flow simulations to investigate how the heterogeneous porosity distribution of the GDL affect overall bulk hydrodynamic properties (*i.e.*, permeability and tortuosity). In order to conduct a parametric study, GDL samples are reconstructed over the entire range of relevant bulk porosity values with homogeneous and heterogeneous porosity profiles. The heterogeneous profile is similar to that reported previously by Fishman et al. [20,21] from CT scan imaging of core section of Toray TGP-H 120™ GDL samples. Furthermore, the effect of the PTFE & binder addition on bulk hydrodynamic properties of GDL samples has also been systematically investigated. PTFE and binder are treated as one solid material.

We have followed the lattice Boltzmann method (LBM) [25] approach for solving the steady-state three-dimensional single-phase fluid flow in the reconstructed geometries. Due to its capability in easily handling complex geometries, the LBM has been used widely to model fluid flow in reconstructed porous structures [17,26–29]. In a recent work, Froning et al. used the same methodology to study the compression effect of the predicted permeability in three-dimensional reconstructed media [30]. In all these works, the porous structure is reconstructed by randomly placing cylindrical fibers in a three-dimensional domain. However, while randomly placing the fibers in the planes, we control the through-plane porosity profile. This enables us to systematically study the effect of porosity heterogeneity on bulk properties. Furthermore, we also investigate the effect of Binder & PTFE addition.

2. Methodology

In this work, steady-state three-dimensional fluid flow was simulated using LBFlow,[1] which is a single-relaxation-time implementation of the LBM [25].

The LBM is a mesoscopic approach for modeling fluid hydrodynamics, where fictitious particles represent fluid volumes. The macroscopic hydrodynamic parameters (*e.g.*, density and velocity) are calculated based on the moments of the distribution function of these fictitious particles on each lattice site. The LBM algorithm includes two steps, namely: (i) streaming step, where the distribution functions move in the direction of their assigned discrete velocity set, and (ii) the collision step, where new distributions are calculated on each lattice site based on pre-defined collision rules. The collision step includes the effect of the external forces and the boundary conditions. The details of the numerical methodology and method validation for LBFlow are presented elsewhere [27,31–33].

The computational domain of the porous region is specified as a three-dimensional binary array of solid and fluid nodes. Physical properties of working fluid are set to those of water at 20 °C. The coordinate system is defined such that the z-direction is aligned with the cross-plane direction, and the x–y plane is the plane parallel to the carbon fibers of the GDLs. A pressure gradient, in the form of a body force, is applied in the direction of each main axis, and the obtained three-dimensional flow field is averaged to yield a volume-averaged velocity vector, $\overline{\boldsymbol{u}}$. The permeability tensor ($\boldsymbol{K}$) is then calculated using Darcy's law, as follows:

$$\overline{u}_i = \frac{K_{ij}}{\mu}\frac{\mathrm{d}p}{\mathrm{d}x_j} \tag{1}$$

where $\overline{u}_i$ is the volume-averaged velocity in the direction i, K_{ij} is the ij^{th} component of the permeability tensor, μ is the working fluid viscosity, and dp/dx_j is the applied pressure gradient in the direction j. Considering the structure of GDL samples in this work, we assumed that off diagonal elements of the permeability tensor (K_{ij}, $I \neq j$) has negligible value in comparison to its diagonal elements (K_{ij}, $I = j$).

[1] Available from http://www.lbflow.co.uk.

Another important bulk property of porous materials is the tortuosity (τ). Tortuosity is usually related to the effective diffusion coefficient (D_{eff}) of porous media as $D_{\text{eff}} = \phi/\tau D$, where D is the binary diffusion coefficient [7]. We used the following formula to calculate the tortuosity in an arbitrary direction i [27]:

$$\tau_i = \frac{\sum u_{\text{mag}}}{\sum u_i} \tag{2}$$

where u_{mag} is the velocity magnitude calculated as $\sqrt{u_x^2 + u_y^2 + u_z^2}$, u_i is the velocity component in direction i, and the summation is performed over all the fluid nodes.

3. Geometry reconstruction

To simulate fluid and mass transport in a GDL-like material, digital models are created using stochastic modeling techniques for fibrous materials. An $Nx \times Ny \times Nz$ voxelized domain is filled with cylinders until a set desired porosity is reached. The sample generation technique that we used in this work most closely resembles that previously reported in Refs. [34,35], but follows similar modeling steps to the family of methods previously applied for digital GDL reconstructions [12,27,36–39]. Similar to [12,39], samples are assumed to be primarily composed of straight, cylindrical fibers, oriented along the primary (x–y) plane of the material, where fibers are allowed to intersect. Additionally, to create heterogeneous samples, the cross-plane porosity distribution of the core section of Toray TGP-H 120™ with 10% wt PTFE [21] is applied to a group of samples, following the methods described in Ref. [40]. The cross-plane, local porosity distribution of a single reconstructed material is displayed in Fig. 1, and compared with the distribution used as input for material generation. The sharp features in generated material's profile are a result of the 0.42 mm^2 sample size, compared to the 25 mm^2 material scanned.

We also created samples with added binder and PTFE. The combination of these two coatings is represented as a secondary material, residing in the tight crevices near fiber intersections, following the methods of [36,39]. The fiber volume percentage, α, is calculated as the ratio of the fibers' volume to the total volume of the solid phase.

Fig. 2 displays three reconstructed samples. Each sample is made to match the same specified cross-plane porosity distribution and have an average bulk porosity of 0.70. However, the fiber to binder & PTFE ratio is varied between the three samples. For a better comparison, the three materials were generated from the same list of fiber positions and orientations, however, those with more binder & PTFE employed a truncated list. In Fig. 2(a), the fiber volume percentage is 50%. In Fig. 2(b), the solid matrix is 75% fibers. Finally, in Fig. 2(c), there is no binder & PTFE at all. Fig. 2(d–f) provide a cross-sectional image of the reconstructed samples. At this cross-plane position, the local porosity is around 0.65. As can be seen from these cross-sections, the inclusion of more fibers creates a higher number of smaller pores. The accumulation of binder & PTFE (marked in blue (in the web version)) at the tight crevices near fiber intersections is visible in Fig. 8(d) and (e).

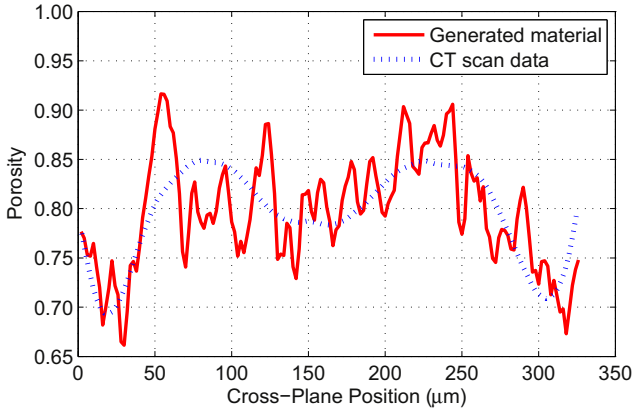

Fig. 1. Comparison between the cross-plane porosity distribution used as input (dashed) to the material generation, and that of a single, 100% fibrous material generated for this study (solid).

Two considerations that were made specifically for the sample reconstructions in this work should be highlighted. First, the fiber placement was done in such a way as to provide ideal sidewall boundaries for periodic simulations. This means that when a sidewall is mated with its opposite face, the boundaries are indistinguishable from the internal volume of the material. To accomplish this feature, individual fiber placement was accomplished in 4 steps:

1) A cylindrical fiber of length Nx is placed in the center of the domain, such that its center point is at $Nx/2$, $Ny/2$, $Nz/2$, extending only in the x-direction.
2) The fiber is translated vertically a random amount, weighted by the intended porosity distribution, as described in Ref. [34].
3) The fiber is then rotated in the x–y plane at a random angle between 0 and 180, about its center point.
4) The fiber is then translated again by a random distance in both the x and y directions, such that the center is moved to another point in the x–y plane, with a uniform probability.
5) Any portion of the fiber that extends past the edge of the domain, is retained, and now extends into the opposite face of the domain, such that if you matched opposite faces together, a straight fiber of length of Nx would be formed.

The size of the reconstructed domain is $Nx = 325$ and $Ny = 325$ lattice units in x and y directions. The sample thickness has changed based on different models, while Nz stays around 150 lattice units typically. The authors have previously studied the effect of domain size on the predicted permeability of porous structures [23]. It has been shown that this domain size is large enough to yield lattice independent results. The fibers are 4 lattice units in diameter. The effect of fiber diameter on the predicted permeability has also been elaborated in a previous work of the authors, where the fiber diameters were systematically changed and predicted permeability was reported [27].

The second consideration that was made for this work pertained to the addition of the binder & PTFE material onto the placed fibers such that a desired porosity distribution would be matched. The porosity distributions used in this work are cross-plane, meaning that the local porosity of the generated samples should be a function of the z coordinate alone. Because the binder & PTFE is placed as a wetting fluid, it disproportionally resides in regions of low porosity. Therefore, although this scheme provides global control of how much binder & PTFE gets added to the sample, there is no local control for binder & PTFE placement. To remedy this, the z-position weighting function ($f(z)$) for random fiber placement is modified. The original function of:

$$f(z) = 1 - \phi(z) \tag{3}$$

where ϕ is the porosity, assumes all material in the sample will be placed in that fashion. We investigated a general function, f^i, that could provide an appropriate weighting for cross-plane fiber placement, while accounting for the fiber to binder & PTFE ratio, α, as well. As a result of the investigation, it was apparent that not only α, but also the shape of the original function, f, played an important

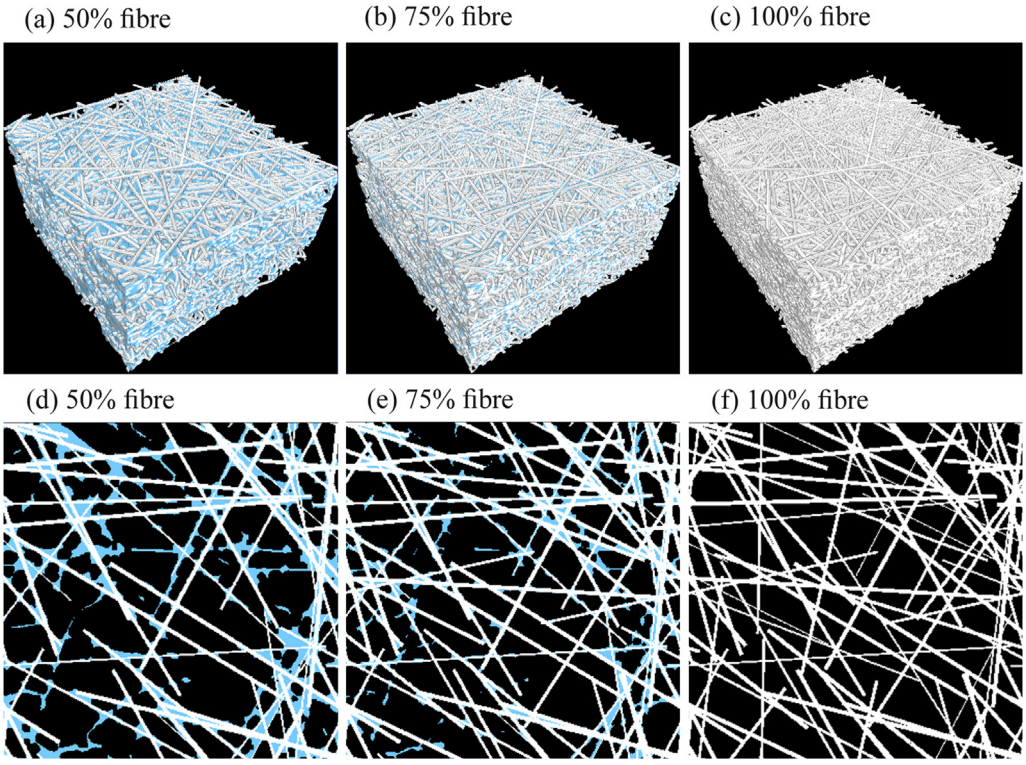

Fig. 2. (Top) three-dimensional structure and (bottom) two-dimensional slices of reconstructed GDL samples with three different fiber percentages of 50%, 75%, and 100%. The color blue shows the added binder & PTFE material, while the white color is representative of fibers. Average bulk porosity of all three samples is 0.70, while the local porosity of the shown slices is around 0.65. (a) 50% fiber; (b) 75% fiber; (c) 100% fiber; (d) 50% fiber; (e) 75% fiber; (f) 100% fiber. (For interpretation of the references to color in this figure legend, the reader is referred to the web version of this article.)

role. Although no general function was found, through trial and error, a relatively good approximation of f' was arrived at using the following function:

$$f'(z) \cong f(z)\left(\frac{\left[\bar{f} - f(z)\right]}{1.5} + 1\right) \tag{4}$$

4. Results

4.1. Introduction

We used a pore-level flow modeling approach to study the effect of simulated GDLs' structure on their hydrodynamic bulk properties, namely: permeability and tortuosity. Two main structural features of GDL samples are investigated in detail. First, effect of porosity heterogeneity on the overall permeability and tortuosity of samples is studied. Second, the effect of the addition of binder & PTFE material on the bulk properties is studied for different values of fiber percentage.

4.2. Effect of porosity heterogeneity in fiber-only samples

In order to study the effect of porosity distribution on the predicted permeability and tortuosity of reconstructed GDL samples, we created samples of homogeneous and heterogeneous porosity distributions in the through-plane direction for the entire range of relevant porosity, *i.e.*, bulk porosities between 0.50 and 0.95. For the heterogeneous samples, we chose the core region of the porosity profile of Toray TGP-H 120™ with 10% wt. PTFE samples, as reported in Ref. [21]. This profile was chosen as it provides the most accentuated porosity heterogeneity, among all the samples that were reported in Refs. [20,21]. At this stage, all the samples consist of only fibers and no secondary material (*i.e.*, binder & PTFE) is added.

The normalized predicted values of in- and cross-plane permeability for homogeneous and heterogeneous GDL samples are presented in Fig. 3. The permeability values are normalized by the square of fibers' radius. It can be seen that for the in-plane permeability, porosity heterogeneity increases the overall permeability of the sample; consistent with what previously discussed in Ref. [22]. However, for the cross-plane direction, the porosity heterogeneity decreases the overall permeability of the samples. One

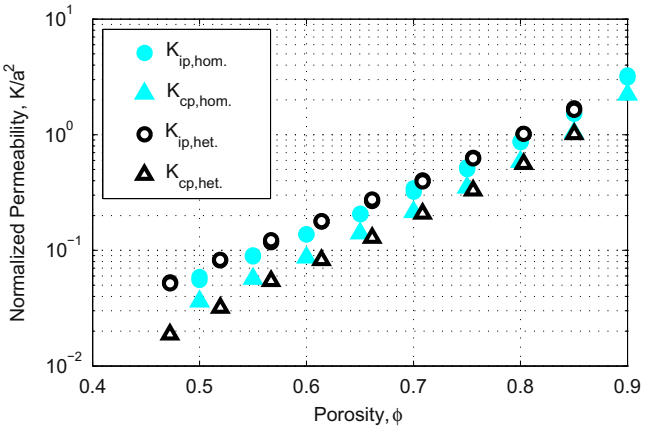

Fig. 3. Predicted values of normalized in- and cross-plane permeability of homogeneous and heterogeneous reconstructed GDL-like samples as a function of porosity.

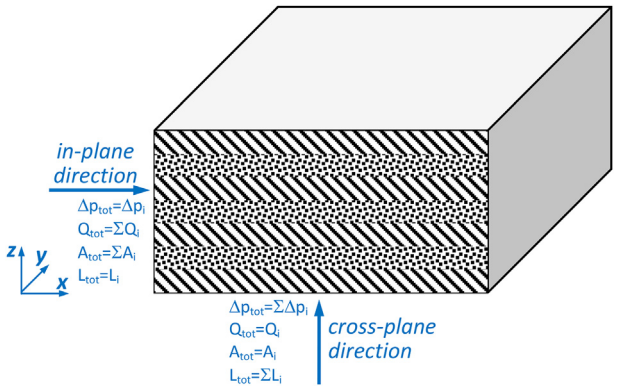

Fig. 4. Schematic of imaginary parallel layers that are used to analytically predict in- and cross-plane permeability of heterogeneous GDL-like samples.

should not that, although the effect of porosity heterogeneity is consistent for the entire range of porosity, it is however negligible compared to the effect of other parameters, such as porosity and fiber aspect ratio [27].

In an attempt to analytically predict the effective permeability of heterogeneous samples from their porosity profile, we assume the GDL is made up of parallel layers, as schematically shown in Fig. 4. These imaginary planes are supposed to be homogeneous, with a uniform porosity corresponding to their respective location on the cross-plane porosity profile. Knowing the porosity of each layer, its permeability can be calculated using available relations in the literature.

For each layer, one can write the Darcy's law as $Q_i = u_i A_i \ [K_i \Delta P_i / \mu L_i] A_i$ for either in-plane or cross-plane directions. Q_i and u_i are the flow rate and average velocity through layer i in the direction of interest. K_i and ΔP_i are the permeability and pressure drop, both in the direction of the mean flow. L_i is the length of the layer i in the direction of mean flow, and μ is the dynamic viscosity of the working fluid. A_i is the cross section of the layer i normal to the direction of interest. It should be noted that as each layer is supposed to be homogeneous, the K_i is the same in all directions.

For the in-plane direction, one can easily observe that $\Delta P_{tot} = \Delta P_i$, $Q_{tot} = \sum Q_i$, $A_{tot} = \sum A_i$, and $L_{tot} = L_i$. Therefore, the overall in-plane permeability can be obtained as a function of the permeability of n imaginary layers that are stacked on top of each other, as follows:

$$K_{ip} = \frac{1}{n} \sum_{i=1}^{n} K_i \tag{5}$$

where n is the number of layers.

For the cross-plane direction, flow direction is normal to the planes, and thus, one can see that $\Delta P_{tot} = \sum \Delta P_i$, $Q_{tot} = Q_i$, $A_{tot} = A_i$, and $L_{tot} = \sum L_i$. Therefore, the overall cross-plane permeability is calculated as follows:

$$K_{cp} = \frac{n}{\sum_{i=1}^{n} (1/K_i)} \tag{6}$$

Table 1 presents a comparison of the numerically predicted values of in- and cross-plane permeability against those predicted from Eqs. (5) and (6) for two representative porosities of 0.75 and 0.85. We used the relationship of Nabovati et al. [27] to predict the permeability of each layer using its corresponding porosity. It can be seen that above-mentioned relations can reasonable predict the permeability of heterogeneous samples, if the permeability of each imaginary layer is correlated to its porosity using available relations in the literature.

Table 1
Comparison of the numerically predicted in- and cross-plane permeability values against those predicted from Eqs. (5) and (6) and relationship of Nabovati et al. [26] for two representative porosities of 0.71 and 0.80.

Overall porosity	K_{ip}		K_{cp}	
	Numerical	Analytical, Eq. (5)	Numerical	Analytical, Eq. (6)
0.71	6.38×10^{-12}	5.52×10^{-12}	3.33×10^{-12}	3.77×10^{-12}
0.80	16.11×10^{-12}	15.04×10^{-12}	8.96×10^{-12}	9.88×10^{-12}

The predicted values of tortuosity for samples of homogeneous and heterogeneous porosity distributions are shown in Fig. 5 as a function of porosity. It can be seen that the cross-plane tortuosity values are consistently larger than the in-plane tortuosity values for both homogeneous and heterogeneous porosity distributions. This behavior is opposite to that of permeability values. Furthermore, it can be seen that the heterogeneity of porosity distribution increases the cross-plane tortuosity and decreases the in-plane tortuosity. However, similar to the predicted values of permeability in Fig. 3, the effect of porosity distribution on the predicted values of tortuosity is negligible in comparison to the effect of fibers' direction (cross-plane vs. in-plane) and porosity.

4.3. Effect of binder & PTFE

In this section, we study the effect of the addition of binder & PTFE to the base fibrous structure of GDLs on the predicted permeability and tortuosity values.

Fig. 6 shows the normalized predicted values of in- and cross-plane permeability as a function of porosity for three different fiber volume percentages of 50, 75, and 100%. It can be seen that for both directions, decreasing the fiber percentage (adding more binder & PTFE) increases the permeability. The effect of fiber percentage on permeability is consistent over the entire range of examined porosity.

The positive effect of adding binder & PTFE on the permeability can be explained considering the difference in geometrical shapes of fibers and binder & PTFE materials, as shown in Fig. 2. Fibers are in the form of straight long circular cylinders; while the added binder & PTFE materials are more in the form of bulk of materials accumulated at the intersection of fibers in a usually irregular bulk-like form. The fibers, thus, have a higher specific surface area (surface area per unit volume) than the added binder & PTFE

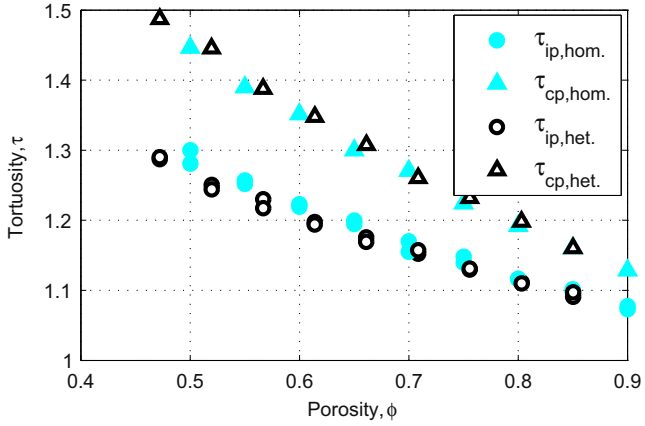

Fig. 5. Predicted values of overall in- and cross-plane tortuosity for homogeneous and heterogeneous reconstructed GDL-like samples.

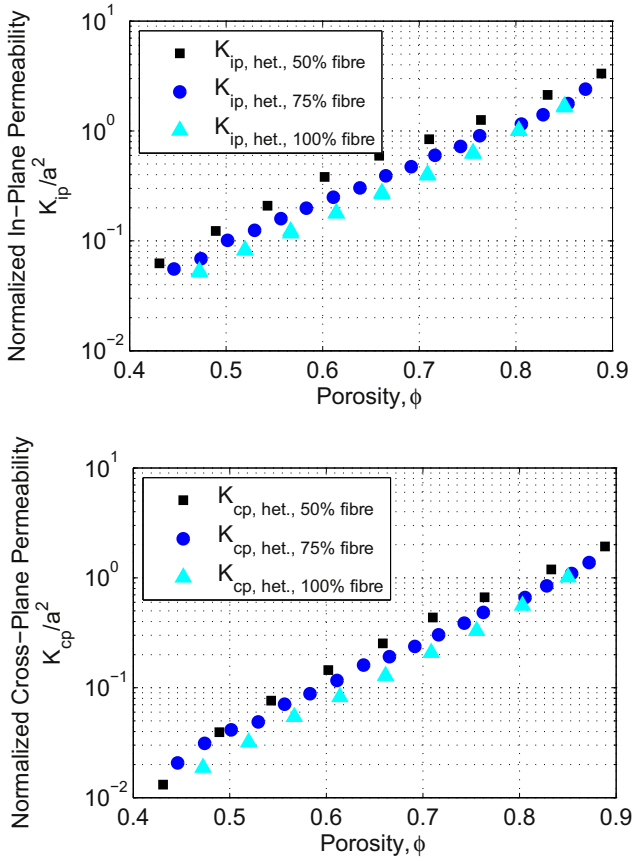

Fig. 6. Predicted values of normalized in-plane (top) and cross-plane (bottom) permeability of reconstructed GDL samples with heterogeneous porosity distribution and three different fiber percentages of 50%, 75%, and 100%.

material. Samples of the same porosity but of different volume percentages of fibers will all have the same volume of materials; however, because of different specific surface area, those with a higher fiber volume percentage (lower binder & PTFE volume percentage) will have a higher solid surface area that is exposed to the working fluid. The reduction in the permeability is mainly because of the friction between the solid material and the flowing fluid. Thus, a higher specific surface area, means a larger surface for friction to act, which results in a lower permeability.

To quantify the effect of fiber volume percentage on the predicted permeability values, we modify a previously reported relation for the permeability of three-dimensional random fibrous structures by Nabovati et al. [27]:

$$\frac{K}{a^2} = C_1\left(\sqrt{\frac{1-\phi_c}{1-\phi}}-1\right)^{C_2} \tag{7}$$

Table 2
Predicted values of C_1 in Eq. (7) for in- and cross-plane directions for different values of fiber volume percentage from curve fitting to the numerically predicted values of permeability for samples with porosities smaller than 0.85. ϕ_c and C_2 are constant and equal to those reported by Nabovati et al. [26], *i.e.*, $\phi_c = 0.074$ and $C_2 = 2.310$.

	In-plane	Cross-plane
50% fiber volume	1.1480	0.6220
75% fiber volume	0.8183	0.4625
100% fiber volume	0.7057	0.3806
Nabovati et al. [26]	0.491	

where a is the fiber radius, ϕ is porosity, and ϕ_c is the percolation threshold. C_1 and C_2 are two fitting parameters related to the geometry of the porous material. The form of this relation was initially proposed by Gebart [41] for the permeability of ordered two-dimensional arrangement of cylinders.

The reported values of ϕ_c, C_1, and C_2 for three-dimensional fibrous porous materials with random structure are 0.074, 0.491, and 2.310, respectively [27]. In this work, the fibers of reconstructed GDL samples have a preferred direction, thus, permeability is different in the in- and cross-plane directions, where both are also different from permeability of random fibrous structures.

In fitting the Eq. (7) to our numerically predicted data, we keep the values of ϕ_c and C_2 constant and equal to those previously reported for random fibrous structure. New values of C_1 for in- and cross-plane directions for three different values of fiber volume percentage are predicted from curve fitting, and are presented in Table 2. As the behavior of samples at the high porosity end is erratic, we only include samples of porosities smaller than 0.85 in the curve fitting process.

Fig. 7 shows the effect of fiber percentage on the predicted values of in- and cross-plane tortuosity. Decreasing the fiber percentage (adding more binder & PTFE) increases the predicted values of tortuosity. The effect of fiber percentage on tortuosity values is more intensified at low porosities, and is almost negligible for porosities larger than 0.80.

The increase in the tortuosity by increasing the volume percentage of binder & PTFE (decreasing the fiber volume percentage) can also be explained by considering the shape of fibers and binder & PTFE material. Large bulk volumes of binder & PTFE material

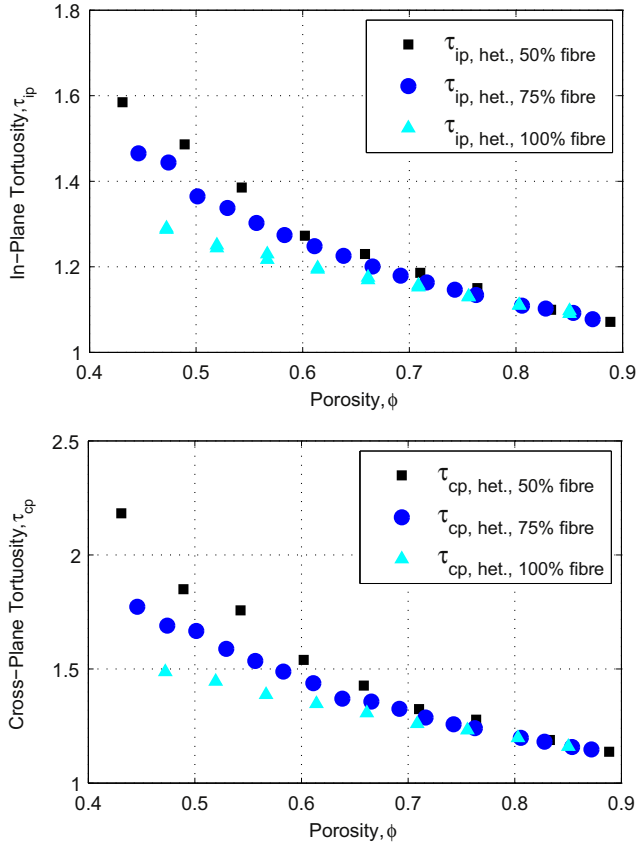

Fig. 7. Predicted values of in-plane (top) and cross-plane (bottom) tortuosity of reconstructed GDL-like samples with heterogeneous porosity distribution and three different fiber percentages of 50%, 75%, and 100%.

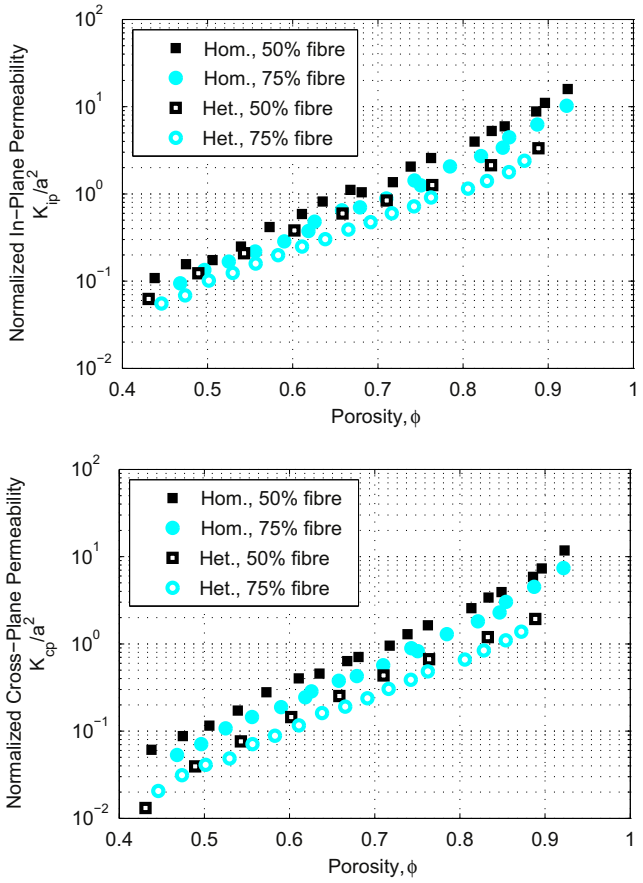

Fig. 8. Effect of porosity heterogeneity on the predicted values of normalized in-plane (top) and cross-plane (bottom) permeability of reconstructed GDL samples with heterogeneous and homogeneous porosity distributions, and two different fiber percentages of 50% and 75%.

distort the flow pattern and streamlines more than the slim fibers, thus, increase the tortuosity of fluid motion.

4.4. Effect of porosity heterogeneity in samples with binder & PTFE

In Section 4.2, we studied the effect of porosity heterogeneity on samples consisting of only fibers. In this section, we study this effect in samples with two different fiber volume percentages of 50 and 75%. Fig. 8 shows the predicted values of in- and cross-plane permeability for samples with homogeneous and heterogeneous distributions of porosity and two different fiber volume percentages. It can be seen that for both in- and cross-plane directions, and for both volume percentages of fibers, the permeability of heterogeneous samples is consistently lower than homogeneous samples for the entire range of the examined porosity.

4.5. Comparison with experimental measurements

In order to validate the methodology and have a comparison with previously reported values of permeability of different GDL samples, we compared the numerically predicted in- and cross-plane permeability values of samples with three different fiber volume fractions against some of the available experimental data in the literature (Fig. 9) [14–16,19,38,42–45]. As some of the experimental works have not reported the radius of fibers in their experimental samples, we have reported the absolute values of permeability. It can be seen that for both in- and cross-plane directions, the numerically predicted values are in very good agreement with the experimentally measured values. One should note the scatter in the experimentally reported data and the linear scale of the vertical axis.

5. Conclusions

We used a pore-level numerical modeling approach to investigate the effect of porosity, porosity distribution, and the volume percentage of binder & PTFE material on the bulk hydrodynamic properties of reconstructed GDL-like samples. It was shown that the effect of porosity heterogeneity is negligible in comparison to the other two factors for all the samples studied here, which are porosity and fiber volume percentage.

Increasing the volume percentage of binder & PTFE in the structure (reducing the fiber percentage) increases both in- and cross-plane permeability and tortuosity values. A previously reported relation for the permeability of fibrous porous materials was adopted and fitted to the predicted values of in- and cross-plane permeability for three different fiber volume percentages. The magnitude of a fitting parameter in that relation was reported as a function of fiber volume percentage. The predicted values of in- and cross-plane permeability show a very good agreement with the available experimental data in the literature.

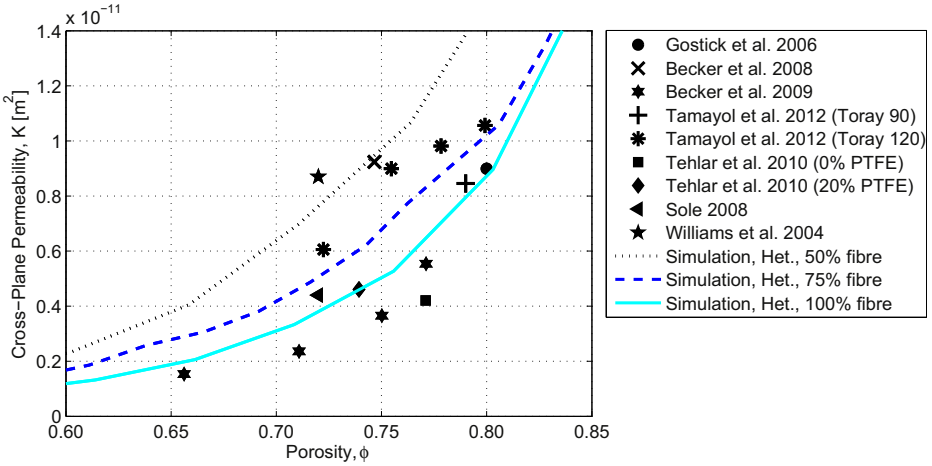

Fig. 9. Comparison of the numerically predicted values of (top) in-plane (bottom) cross-plane permeability of sample with heterogeneous porosity distribution and three different fiber percentages of 50%, 75%, and 100% against some of the available experimental data in the literature.

Acknowledgments

AN and CA acknowledge the financial support from Mitacs, Natural Sciences and Engineering Research Council of Canada (NSERC), and Ballard Power Systems. JH and AB acknowledge the financial support from NSERC, Canada Foundation for Innovation (CFI), the Hatch Scholarship for Sustainable Energy Research, and the University of Toronto.

The authors thank Dr. Edward W. Llewellin (Durham University) for helpful discussions and providing the computational code. Computations were performed on the GPC supercomputer at the SciNet HPC Consortium. SciNet is funded by: the Canada Foundation for Innovation under the auspices of Compute Canada; the Government of Ontario; Ontario Research Fund - Research Excellence; and the University of Toronto.

References

[1] N. Djilali, Energy 32 (4) (2007) 269–280.
[2] J.-H. Wee, Renew. Sustain. Energy Rev. 11 (8) (2007) 1720–1738.
[3] S.K. Das, A.S. Bansode, Heat Transf. Eng. 30 (9) (2009) 691–719.
[4] L. Zhang, S.-R. Chae, Z. Hendren, J.-S. Park, M.R. Wiesner, Chem. Eng. J. 204–205 (2012) 87–97.
[5] H. Li, Y. Tang, Z. Wang, Z. Shi, S. Wu, D. Song, J. Zhang, K. Fatih, J. Zhang, H. Wang, Z. Liu, R. Abouatallah, A. Mazza, J. Power Sources 178 (1) (2008) 103–117.
[6] A. El-Kharouf, T.J. Mason, D.J.L. Brett, B.G. Pollet, J. Power Sources 218 (2012) 393–404.
[7] L. Cindrella, A.M. Kannan, J.F. Lin, K. Saminathan, Y. Ho, C.W. Lin, J. Wertz, J. Power Sources 194 (1) (2009) 146–160.
[8] M. Khandelwal, M.M. Mench, J. Power Sources 161 (2) (2006) 1106–1115.
[9] E. Sadeghi, M. Bahrami, N. Djilali, J. Power Sources 179 (1) (2008) 200–208.
[10] N. Zamel, X. Li, J. Shen, J. Becker, A. Wiegmann, Chem. Eng. Sci. 65 (13) (2010) 3994–4006.
[11] J. Yablecki, A. Nabovati, A. Bazylak, J. Electrochem. Soc. 159 (6) (2012) B647–B653.
[12] J. Yablecki, J. Hinebaugh, A. Bazylak, J. Electrochem. Soc. 159 (12) (2012) F805–F809.
[13] J. Yablecki, A. Bazylak, J. Power Sources 217 (2012) 470–478.
[14] J.P. Feser, A.K. Prasad, S.G. Advani, J. Power Sources 162 (2 spec. iss.) (2006) 1226–1231.
[15] J.T. Gostick, M.W. Fowler, M.D. Pritzker, M.A. Ioannidis, L.M. Behra, J. Power Sources 162 (1) (2006) 228–238.
[16] J. Becker, R. Flckiger, M. Reum, F.N. Bchi, F. Marone, M. Stampanoni, J. Electrochem. Soc. 156 (10) (2009) B1175–B1181.
[17] L. Hao, P. Cheng, J. Power Sources 186 (1) (2009) 104–114.
[18] T. Munekata, T. Inamuro, S. Hyodo, Commun. Comput. Phys. 9 (5) (2011) 1335–1346.
[19] A. Tamayol, F. McGregor, M. Bahrami, J. Power Sources 204 (2012) 94–99.
[20] Z. Fishman, J. Hinebaugh, A. Bazylak, J. Electrochem. Soc. 157 (11) (2010) B1643–B1650.
[21] Z. Fishman, A. Bazylak, J. Electrochem. Soc. 158 (8) (2011) B841–B845.
[22] D.A. Nield, A. Bejan, Convection in Porous Media, Springer Verlag, New York, 1999.
[23] A. Nabovati, C.H. Amon, Transp. Porous Media 96 (1) (2013) 83–95.
[24] Z. Fishman, A. Bazylak, J. Electrochem. Soc. 158 (2) (2011) B247–B252.
[25] S. Succi, The Lattice Boltzmann Equation for Fluid Mechanics and Beyond, Oxford University Press, Oxford, 2001.
[26] X.-D. Niu, T. Munekata, S.-A. Hyodo, K. Suga, J. Power Sources 172 (2007) 542–552.
[27] A. Nabovati, E.W. Llewellin, A.C.M. Sousa, Compos. Part A Appl. Sci. Manuf. 40 (6–7) (2009) 860–869.
[28] Y. Gao, X. Zhang, P. Rama, R. Chen, H. Ostadi, K. Jiang, J. Fuel Cell Sci. Technol. 9 (2012) 041010-1–041010-10.
[29] L. Chen, H.-B. Luan, Y.-L. He, W.-Q. Tao, Int. J. Therm. Sci. 51 (2012) 132–144.
[30] D. Froning, J. Brinkmann, U. Reimer, V. Schmidt, W. Lehnert, D. Stolten, Electrochim. Acta (2013) in press.
[31] A. Nabovati, E.W. Llewellin, A.C.M. Sousa, Compos. Part A Appl. Sci. Manuf. 41 (4) (2010) 453–463.
[32] E.W. Llewellin, Comp. Geosci. 36 (2) (2010) 115–122.
[33] E.W. Llewellin, Comp. Geosci. 36 (2) (2010) 123–132.
[34] J. Hinebaugh, A. Bazylak, in: ASME 2011 5th International Conference on Energy Sustainability & 9th Fuel Cell Science, Engineering and Technology Conference, ESFuelCell2011, 2011, p. 54422.
[35] J. Hinebaugh, A. Bazylak, in: ASME 2012 6th International Conference on Energy Sustainability & 10th Fuel Cell Science, Engineering and Technology Conference, ESFuelCell2012, 2012, p. 91466.
[36] V.P. Schulz, J. Becker, A. Wiegmann, P.P. Mukherjee, C.Y. Wang, J. Electrochem. Soc. 154 (4) (2007) B419–B426.
[37] G. Inoue, T. Yoshimoto, Y. Matsukuma, M. Minemoto, J. Power Sources 175 (1) (2008) 145–158.
[38] J. Becker, V. Schulz, A. Wiegmann, J. Fuel Cell Sci. Technol. 5 (2) (2008) 021006.
[39] M.M. Daino, S.G. Kandlikar, Int. J. Hydrogen Energy 37 (6) (2012) 5180–5189.
[40] J. Hinebaugh, Z. Fishman, A. Bazylak, J. Electrochem. Soc. 157 (11) (2010) B1651–B1657.
[41] B.R. Gebart, J. Compos. Mater. 26 (8) (1992) 1100–1133.
[42] M.V. Williams, H. Russell Kunz, J.M. Fenton, J. Electrochem. Soc. 151 (10) (2004) A1617–A1627.
[43] J.D. Sole, Investigation of Water Transport Parameters and Processes in the Gas Diffusion Layer of PEM Fuel Cells. PhD dissertation, Virginia Polytechnic Institute and State University, Blacksburg, VA, 2008.
[44] D. Tehlar, R. Flckiger, A. Wokaun, F.N. Bchi, Fuel Cells 10 (6) (2010) 1040–1049.
[45] I.S. Hussaini, C.Y. Wang, J. Power Sources 195 (12) (2010) 3830–3840.